Shallow seismic trapping structure in the San Jacinto fault zone near Anza, California

M. A. Lewis,[1]* Z. Peng,[1]† Y. Ben-Zion[1] and F. L. Vernon[2]

[1]*Department of Earth Sciences, University of Southern California, Los Angeles,* CA, 90089-0740, *USA. E-mail: malewis@usc.edu*
[2]*Institute of Geophysics and Planetary Physics, Scripps Institution of Oceanography, University of California, San Diego,* 9500 *Gilman Drive, La Jolla,* CA 92093-0225, *USA*

SUMMARY
We analyse fault zone trapped waves, generated by ∼500 small earthquakes, for high-resolution imaging of the subsurface structure of the Coyote Creek, Clark Valley and Buck Ridge branches of the San Jacinto fault zone near Anza, California. Based on a small number of selected trapped waves within this data set, a previous study concluded on the existence of a low-velocity waveguide that is continuous to a depth of 15–20 km. In contrast, our systematic analysis of the larger data set indicates a shallow trapping structure that extends only to a depth of 3–5 km. This is based on the following lines of evidence. (1) Earthquakes clearly outside these fault branches generate fault zone trapped waves that are recorded by stations within the fault zones. (2) A traveltime analysis of the difference between the direct *S* arrivals and trapped wave groups shows no systematic increase (moveout) with increasing hypocentral distance or event depth. Estimates based on the observed average moveout values indicate that the propagation distances within the low-velocity fault zone layers are 3–5 km. (3) Quantitative waveform inversions of trapped wave data indicate similar short propagation distances within the low-velocity fault zone layers. The results are compatible with recent inferences on shallow trapping structures along several other faults and rupture zones. The waveform inversions also indicate that the shallow trapping structures are offset to the northeast from the surface trace of each fault branch. This may result from a preferred propagation direction of large earthquake ruptures on the San Jacinto fault.

Key words: earthquake dynamics, guided waves, inversion, San Jacinto fault, velocity model, waveform analysis.

GJI Seismology

1 INTRODUCTION

1.1 Geological setting and trapped wave characteristics

The San Jacinto fault zone (SJFZ) is one of the most active fault zones (FZs) in southern California (e.g. Sanders & Kanamori 1984). It extends ∼230 km southeastwards from the San Gabriel Mountains to the Salton Trough at its southern extent (inset of Fig. 1). The cumulative slip across the SJFZ is estimated at around 24 km (Sharp 1967) and 29 km (Scott *et al.* 1994) over about 2 million years. Large faults that have accommodated such significant slip typically generate zones of intensely damaged material with lower seismic velocity than the surrounding rocks (Ben-Zion & Sammis

2003, and references therein). If spatially persistent and sufficiently uniform, the low-velocity FZ rock can act as a waveguide for seismic energy. The constructive interference of critically reflected phases, which are generated within a low-velocity layer and arrive after the *S* waves, are generally termed as FZ trapped waves (e.g. Ben-Zion & Aki 1990; Li *et al.* 1990; Ben-Zion 1998). Since the amplitude and frequency content of the trapped waves depend strongly on the properties of the FZ waveguide within which they propagate, FZ trapped waves can provide high-resolution information on geometrical and seismic properties of the FZ waveguide at depth.

Various previous FZ trapped wave studies relied on a small number of selected waveforms in drawing conclusions on approximately 100-m wide low-velocity FZ layers that extend to the base of the seismogenic zone (e.g. Li & Leary 1990; Li *et al.* 1990, 1997). Li & Vernon (2001) recorded about 1500 small earthquakes on FZ arrays located across the Buck Ridge (BR), Clark Valley (CL) and the Coyote Creek (CC) branches of the SJFZ near Anza, California. They identified FZ trapped waves on the three fault branches from a small waveform subset of 25 on-fault events and 1 off-fault event.

*Corresponding author: Department of Earth Sciences, University of Southern California, Los Angeles, CA 90089-0740, USA.
†Now at: Department of Earth and Space Sciences, University of California, Los Angeles, CA, 90095, USA.
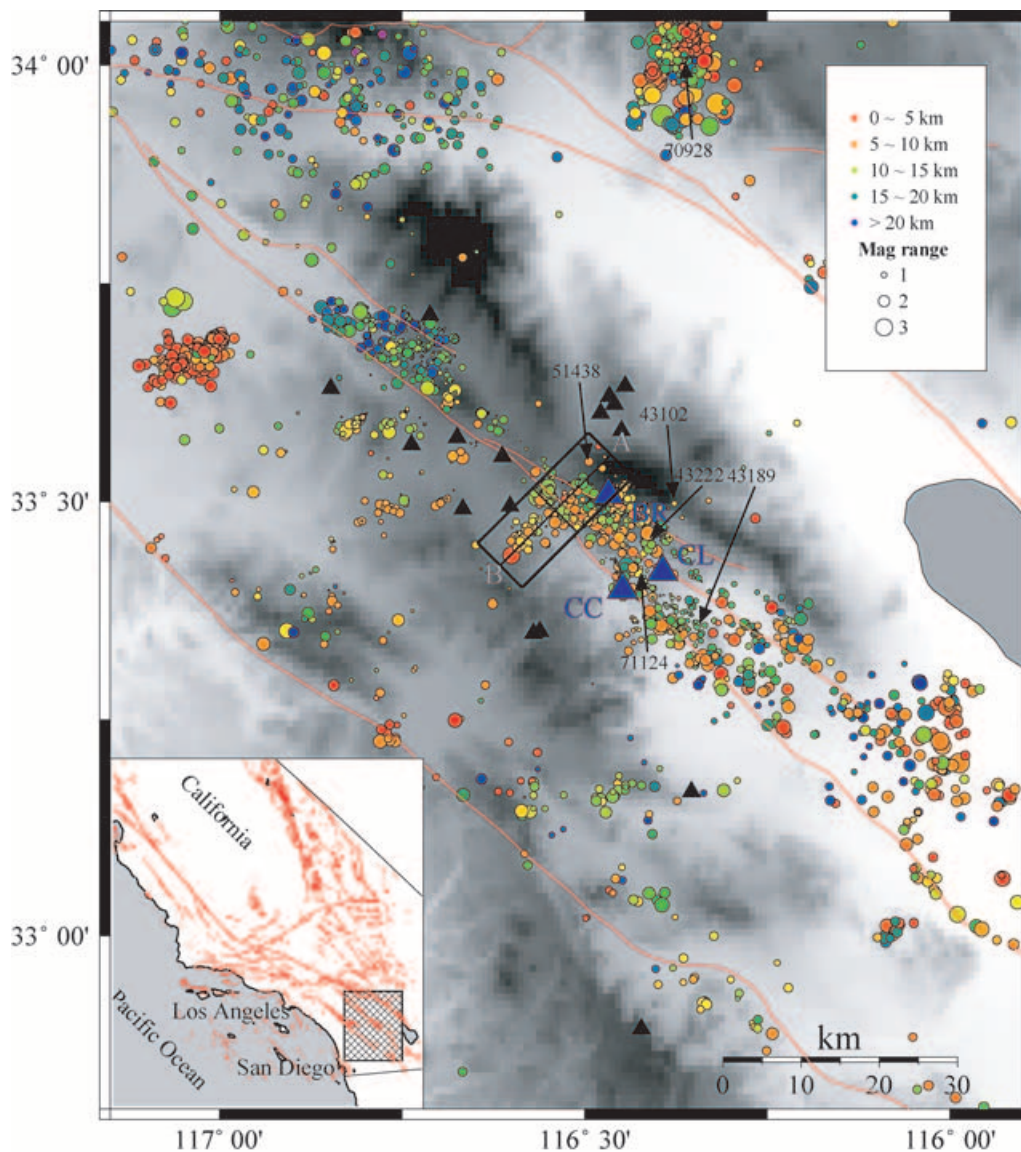
Figure 1. A map of the San Jacinto fault in southern California. Black triangles represent stations in the Anza seismic network. The enlarged blue triangles show the locations of the three dense FZ arrays. Circles denote events that are located by the Anza network during the operation period of the dense arrays. The size of each circle is scaled with the event magnitude and is colour coded with depth. The red lines denote the surface traces of the SJFZ and other major faults in Southern California. Events marked by arrows are plotted in Figs 3–5. The inset shows a broader view of the study area. The cross-section A–B marked by a box is used in Figs 10 and 11.

The FZ structures were modelled as waveguides that are continuous to the base of the seismicity (∼18 km) and have depth-varying properties (width of 75–100 m, shear wave velocity reduction of 20–30 per cent from that of the surrounding rock, and Q values of 40–90). They further inferred that the BR FZ dips to the southwest to join with the northeastward dipping CL FZ at depth. The CC fault was inferred as near vertical and unconnected to the others. Igel *et al.* (1997) and Jahnke *et al.* (2002) showed with extensive 3-D numerical simulations that smoothly varying width and velocity with depth, as well as other internal variations on a scale smaller than the FZ width, are not resolvable parameters from trapped waves. In a continuous waveguide structure, FZ trapped waves are sensitive only to the average properties of the waveguide. Thus, the models derived by Li & Vernon (2001) include many details that cannot be resolved reliably from analysis of trapped waves. In this work, we perform systematic analysis of a much larger data set, modelling quantita-

tively trapped waves data with a considerably simpler model having only parameters that are sensitive degrees of freedom of trapped waves.

Igel *et al.* (2002), Jahnke *et al.* (2002) and Fohrmann *et al.* (2004) showed that a shallow FZ layer can trap seismic energy from events that are deeper than and well outside the FZ. In contrast, a FZ waveguide that is continuous with depth can only trap seismic waves of events very close to or within the FZ layer. Constraining the FZ structures thus requires a systematic analysis of a large number of broadly distributed events. The use of such large data sets on the San Andreas fault (SAF) at Parkfield (Michael & Ben-Zion 1998; Korneev *et al.* 2003), the rupture zone of the 1992 Landers, California, earthquake (Peng *et al.* 2003), an inactive fault in central Italy (Marra *et al.* 2000; Rovelli *et al.* 2002) and the Karadere-Düzce branch of the North Anatolian fault (NAF) in Turkey (Ben-Zion *et al.* 2003) resulted in conclusions of shallow trapping structures.

In the following sections, we first describe briefly the general aspects of the earthquake data used in this study. Then we assign a quality of trapped wave generation to each earthquake using a spectral ratio method and examine the spatial distribution of the events with high quality. We further analyse the traveltime moveout between body *S* and trapped waves in various cross-sections, and finally perform synthetic waveform modelling of several sets of FZ waves. In contrast to the previous conclusion of waveguides continuous to the bottom of the seismogenic zone in the SJFZ (Li & Vernon 2001), our analysis based on a larger data set indicates that the trapping structures extend only over the (largely aseismic) top 3–5 km of the crust.

2 ANALYSIS

2.1 Data collection

Three dense FZ arrays were deployed across the CC, CL and BR fault branches of the SJFZ south of Anza to record FZ trapped waves from small earthquakes (Li & Vernon 2001). Each array consists of 12 three-component short-period instruments that are aligned vertical, parallel and perpendicular to the fault. Station separation is of the order of 25 m in the centre and ∼50 m near the end, leading to a total array length of ∼350 m. The arrays perpendicular to the BR and CL fault branches were deployed for only 2 months, while the array across the CC fault recorded 6 months of data. During the operational period, waveforms of ∼1500 events within 100 km were recorded by the arrays. In this study, we analyse a subset of ∼500 events that were recorded by at least seven instruments (including the central FZ station) within one of the arrays. The event locations are obtained from the Anza seismic network (e.g. Berger *et al.* 1984). The estimated location errors are less than 1.5 km horizontally and less than 3 km vertically (Fletcher *et al.* 1987). These errors are sufficiently small for the analysis performed in this work. Additional details on the experiment and data set are given by Li & Vernon (2001).

2.2 Spatial distribution of events generating trapped waves

The spatial distribution of earthquakes generating FZ trapped waves provides important constraints on the overall properties of the trapping structure. In previous studies (e.g. Li & Vernon 2001; Ben-Zion *et al.* 2003), the quality of the trapped waves has generally been assigned by visual inspection. However, an automatic method is needed in the analysis of a large number of events. Here we use a spectral ratio technique to automatically assign quality to the FZ trapped waves generation.

The procedure employed is as follows. We first compute the amplitude spectrum of each fault-parallel seismogram over a 2.5-s time window, starting 0.5 s before the *S* arrival (Fig. 2a). The spectra for the seismograms recorded by the stations near the FZ (here station NE1) are divided by the mean spectra of the four stations (two on each end) that are furthest from the centre of the array (Fig. 2b). The area under the resulting spectral ratio in the range 2–12 Hz (Fig. 2c) is normalized by dividing by the frequency range (i.e. 10), and this value is used as a measure of the quality of the trapped waves generated for the event.

Figs 3–5 show examples of seismograms and corresponding spectra generated by events that have high quality of trapped wave generation and are located relatively close to and off the fault. In general, stations close to the surface trace of the faults (marked in bold)

record large-amplitude low-frequency phases after the *S* wave arrival, while these characteristics are much weaker or missing for stations further away from the faults. Figs 3–5(c, d) give contour maps of normalized amplitude spectra versus position of the stations. The concentration of spectral energy between about 4 and 10 Hz within ∼100 m of the surface trace of these faults is associated with FZ trapped waves. The differences of the spectral distributions for events close to and off the faults are smaller than the differences between data recorded by the different arrays, suggesting that the near-station fault structures play an important role in generating the observed FZ trapped waves. We note that the maximum amplitude of trapped waves and corresponding peaks of spectral energy are offset to the NE from the stations located closest to the surface traces of each fault. We return to this issue in later sections.

Fig. 6 shows the locations, coded with the values of spectral ratios, for all events recorded by each of the three arrays. The top 25 per cent, middle 50 per cent and bottom 25 per cent of the spectral ratios for all of the data are assigned, respectively, quality A, B and C for FZ trapped waves generation. In general, events near the faults have higher spectral ratios than those that are further away. However, some events clearly off the faults generate FZ trapped waves with quality A or B. In Section 2.3 we show clear examples of events outside the faults, along the cross-section A–B of Fig. 1, with quality A or B of trapped waves generation (Figs 10a–11a). The observation of events outside the FZ generating considerable trapped wave energy indicates the existence of a shallow trapping structure at these faults. In addition, the overall spectral ratios are higher for the CC array (with a mean value of 1.68) than those for the CL and BR arrays (with mean values of 1.53 and 1.50, respectively), suggesting that the trapping efficiencies for the three faults are different.

One theoretical characteristic of trapped waves is a predominance of motion parallel to the low-velocity FZ layer (Ben-Zion & Aki 1990). Our method of assigning quality of trapped wave generation does not differentiate between trapped waves and other FZ-related site effects. To verify the validity of the method, the obtained quality values are compared with the spectral ratios of the fault-parallel divided by fault-perpendicular components of the near-fault records. The results (Fig. 7) show that as the events' quality increase, so do the ratios of amplification in the fault-parallel motion relative to the fault-perpendicular component. This lends support to our automatic procedure of assigning quality of trapped wave generation.

2.3 Traveltime moveout analysis

To further constrain the depth extent of the trapping structure, we examine the dependence of the traveltime delays, or moveout, between the FZ trapped waves and *S* phases on the propagation distance inside the FZ. For a low-velocity FZ layer in a homogenous half-space (HS), the time difference Δt between the *S* phase and trapped wave group increases with propagation distance r_s in the FZ layer (Ben-Zion *et al.* 2003) as

$$r_s = \frac{2\beta_{HS}\beta_{FZ}}{\beta_{HS} - \beta_{FZ}}\Delta t, \tag{1}$$

where β_{HS} and β_{FZ} are the *S* wave velocity of the HS and FZ, respectively. If the waveguide is continuous, we would expect to see a moveout between the *S* phase and trapped waves for events with increasing propagation distance within the FZ.

Fig. 8(a) shows the fault-parallel seismograms at FZ station CCNE1, generated by events within a 5-km epicentral distance from the station. Most of the events are located inside or close to the CC
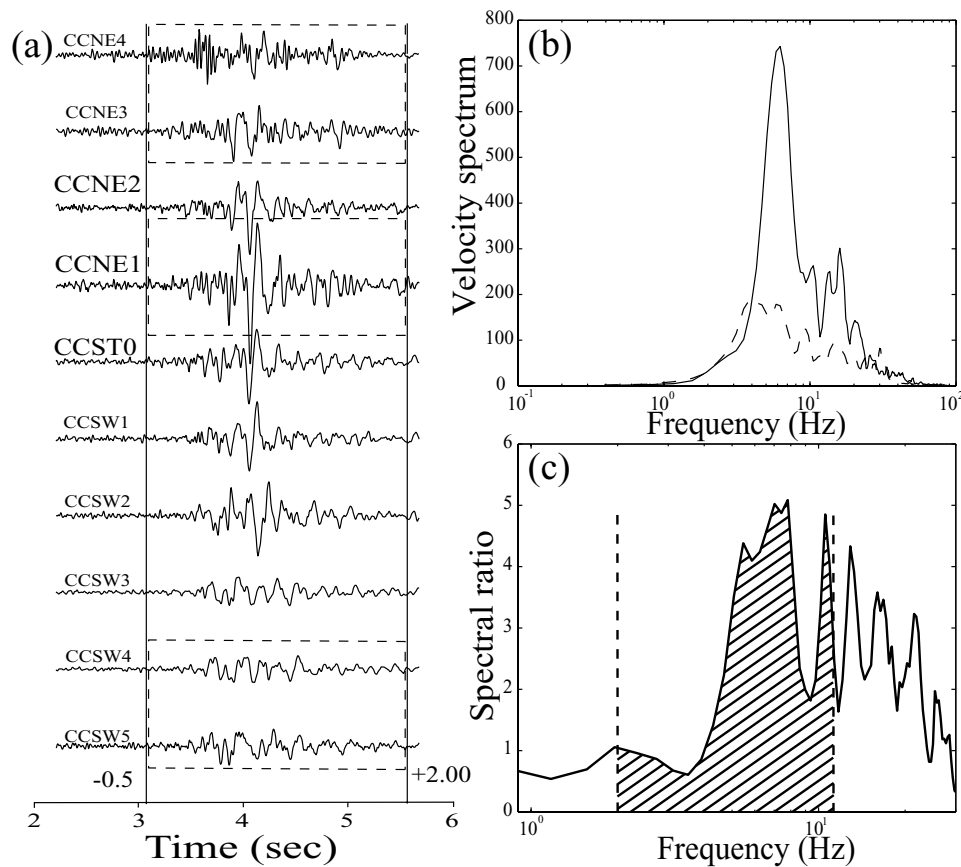
Figure 2. (a) Example of fault-parallel-component seismogram recorded at array CC. The solid vertical lines mark the portion used in the spectral analysis, while the dashed boxes denote the stations used in the spectral ratio calculation. (b) The average velocity spectra recorded at array stations relatively off the fault (dashed) and stations close to the fault (solid). (c) The spectral ratio obtained from the average velocity spectra in (b). The shaded area after normalization is used as a measure of the trapped wave quality.

fault (Figs 8b–c) and are assigned quality A of trapped waves generation. Fig. 8(d) shows the time delay between the *S* arrival and the centre of the trapped wave group as a function of depth. The centre of the trapped wave group is calculated as the mid point between the average time of one oscillation after the *S* arrival and the end of the trapped wave group. The latter are picked by hand on the fault-parallel seismograms as the point when the amplitude reduces to below that of the *S* wave. Clearly, there is no persistent moveout between the *S* and FZ trapped waves with increasing depth. Fig. 9 shows similar results for FZ stations within arrays CL and BR and events located nearby. Again, there is no clear increasing trend between the time delays and hypocentral depths. The results of Figs 8(a–d) and 9 indicate similar propagation distances inside a low-velocity FZ waveguide above the shallowest events at each array.

Figs 10 and 11 give results analogous to those of Figs 8 and 9, but for events generated along the cross-section A–B of Fig. 1. The locations of these events may delineate a cross-fault, which have been suggested to exist in the SJFZ (Mori 1993; Sharp 1967). If we assume a deep and continuous waveguide, then only events inside or close to the damage zone will produce clear FZ trapped waves. Such a continuous waveguide would result in a peak in the quality of trapped waves and time delay for events with zero or small horizontal offset from the fault. However, if a shallow discontinuous waveguide is responsible for generating the trapped waves, then the quality of the trapped waves and the time delay between *S* and trapped waves

will not have a strong dependence on the horizontal offset for events below the trapping structure and at different distances from the fault. The data in Figs 10(c) and 11(c) support the latter interpretation, and again suggest shallow waveguide structures in our study area.

Fig. 12 shows the time delay between the *S* waves and trapped wave groups for all events recorded at each array. For every event where a time delay can be measured, the value is approximately constant and no persistent moveout with distance exists. The variance of the data points does illustrate how using only a selected number of events could lead to the conclusion that a trend with distance exists.

The mean time differences between the *S* phases and trapped waves for all events recorded at the arrays CC, CL and BR are 0.58, 0.52 and 0.58 s, respectively. The synthetic waveform modelling in the next section gives an average *S* wave velocity for the HS of 3 km s^{-1}, and FZ velocities of 1.8 km s^{-1} for the three different branches. Using these values in eq. (1), the propagation distances inside the FZ layer of the CC, CL and BR branches are estimated to be 5.2, 4.7 and 5.2 km, respectively. Since the propagation path of the FZ trapped waves includes both vertical and along-strike components, these values are upper bounds of the depth extent of the waveguides at these faults.

2.4 Synthetic waveform modelling of the FZ waves

The observation of a broad distribution of events generating FZ waves in Section 2.2 suggests that the trapping structure is shallow.
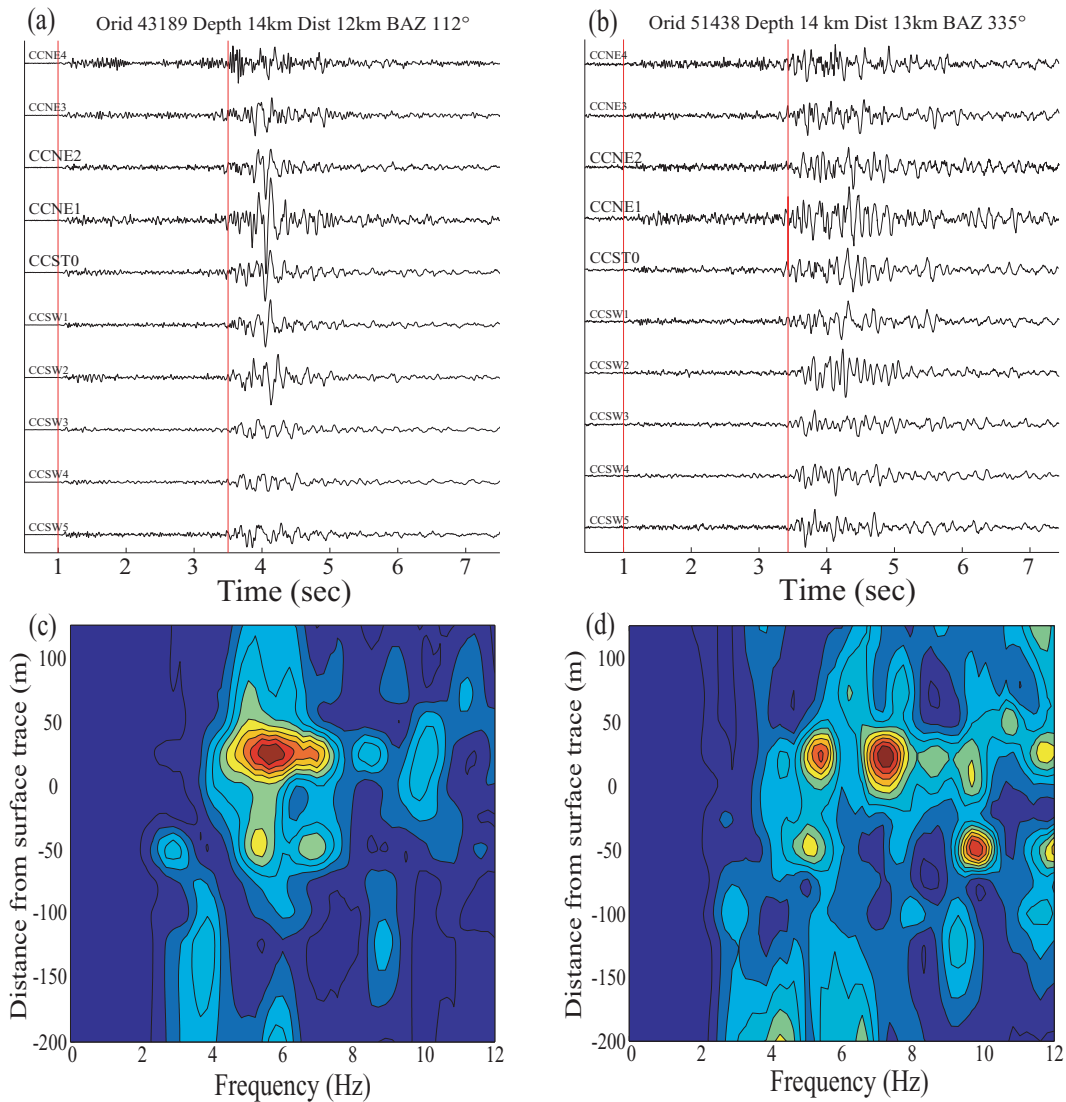
Figure 3. Examples of fault-parallel-component seismograms recorded at array CC and generated by events located relatively close to (a) and off (b) the fault. The event ID, depth, epicentral distance (Dist) and backazimuth (BAZ) are marked on top of each panel. The event locations are shown in Fig. 1. Red vertical bars mark the catalogue picks of the *P* and *S* wave arrivals. The station name is marked on the left hand side of each trace, and stations close to the surface trace are highlighted in bold. (c–d) Normalized amplitude spectra versus position of stations across array CC from waveforms shown in (a–b).

This interpretation is supported in Section 2.3 by a lack of traveltime moveout between the FZ trapped waves and *S* arrivals with respect to increasing propagation distances inside the FZ. To further quantify the seismic properties of the FZ waveguide, we perform synthetic waveform modelling of observed FZ waves using the 2-D analytical solution of Ben-Zion & Aki (1990) for an SH line dislocation with a unit-step source-time function in a plane-parallel layered FZ structure between two quarter spaces. The analysis done here employs a simplified model configuration consisting of a single vertical FZ layer in a surrounding half-space (e.g. Ben-Zion *et al.* 2003). The 2-D analytical solution provides an effective modelling tool for trapped waves in a FZ structure with width much smaller than the length and depth dimensions and larger than the length scale of internal FZ heterogeneities (Igel *et al.* 1997; Jahnke *et al.* 2002; Ben-Zion *et al.* 2003). Previously, using the same model, good waveform fits were obtained for trapped waves observed along the Parkfield section of the SAF (Michael & Ben-Zion 1998), the Karadere-Düzce branch of the NAF (Ben-Zion *et al.* 2003), the rupture zone of the

Landers earthquake (Peng *et al.* 2003) and other locations (Haberland *et al.* 2003; Mizuno *et al.* 2004). While trapped waves are not sensitive to gradual internal variations in the FZ structure, they are *highly* sensitive (Ben-Zion 1998) to changes in the overall average properties of the waveguide. The employed model accounts for these sensitive parameters.

Ben-Zion (1998) showed that there are strong non-orthogonal trade-offs between sets of average 2-D FZ parameters. To quantitatively account for the trade-offs, we model the observed FZ trapped waves recorded at multiple stations using a genetic inversion algorithm (GIA) that employs the 2-D analytical solution as a forward kernel (Michael & Ben-Zion 1998). The free parameters in the inversion are the *S*-wave velocities of the FZ and host rock, the *S*-wave attenuation coefficient of the FZ material, the width and propagation distance inside the FZ layer, the source position and the centre of the FZ layer with respect to the instrument located at the surface trace of the fault. To reduce the number of parameters, we fix the attenuation coefficient of the host rock to be 1000 (e.g. Ben-Zion *et al.* 2003).
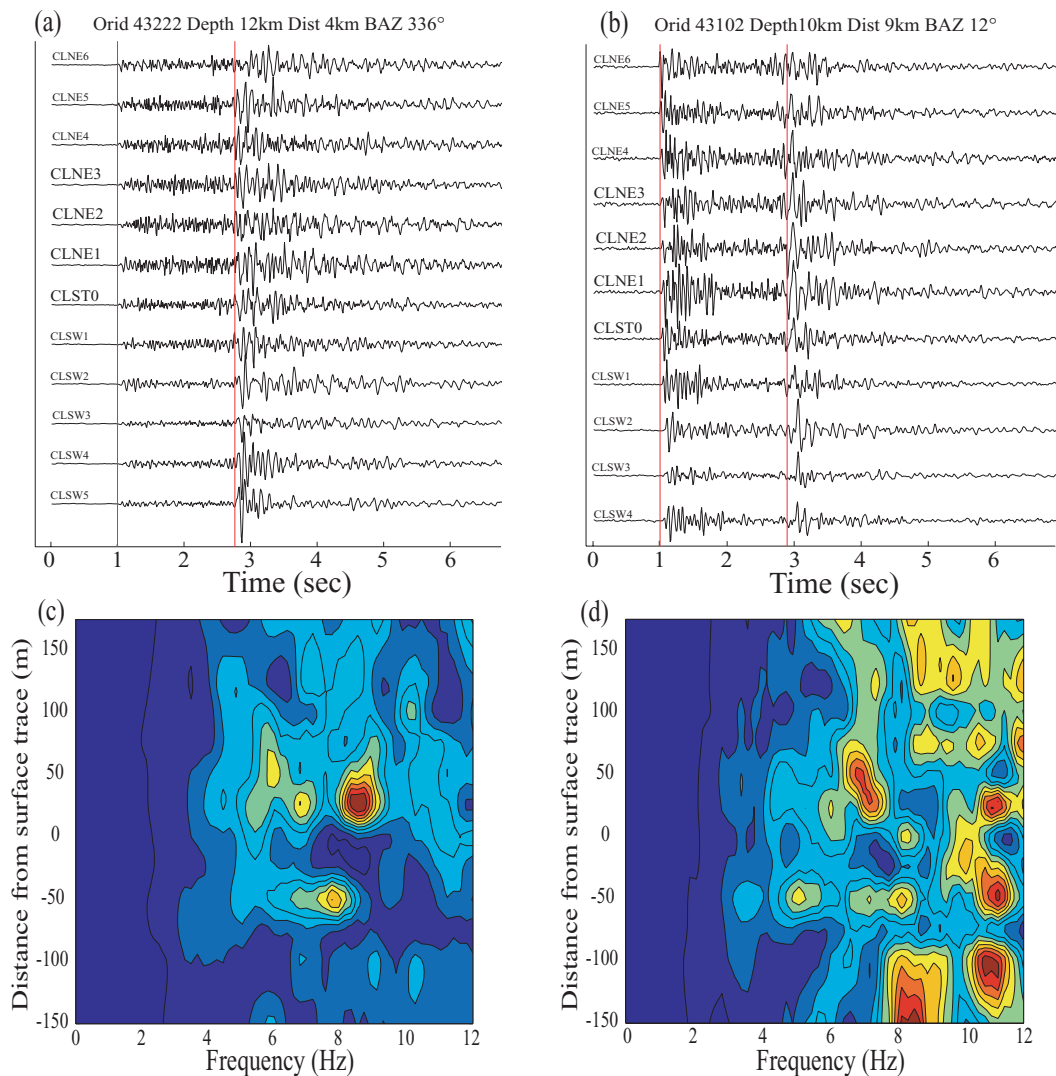
Figure 4. Examples of fault-parallel-component seismograms recorded at array CL and generated by events located relatively close to (a) and off (b) the fault. (c–d) Normalized amplitude spectra versus position of stations across array CL from waveforms shown in (a–b). Other notations are the same as in Fig. 3. The less obvious phase following the *S* wave arrivals in (a–b) and more broadly distributed energy in (c–d) than corresponding results in Fig. 3 suggest a less developed waveguide on this fault branch.

Additional details on the method can be found in Ben-Zion *et al.* (2003).

Prior to the inversion, we remove the instrument response and convert the fault-parallel seismograms into displacement. We also convolve the seismograms with $1/t^{1/2}$ to obtain the equivalent 2-D line-source seismograms (e.g. Igel *et al.* 2002; Ben-Zion *et al.* 2003). Fig. 13(a) shows examples of synthetic waveforms fits for the CC array along with the fitness values calculated by the GIA for different FZ parameters. The fitness for a given set of parameters is defined as $(1 + C)/2$, where C is the cross-correlation coefficient between the employed sets of observed and synthetic waveforms at multiple stations. The thin curves in Fig. 13(b) give probability density functions for the various model parameters, calculated by summing the fitness values of the final 2000 inversion iterations and normalizing the results to have unit sums. The synthetic waveforms fits were generated using the best-fitting parameters associated with the highest fitness values during 10 000 iterations. The ranges of parameters with relatively high fitness values provide estimates for the errors associated with the best-fitting parameters. Figs 14 and 15

show corresponding waveform modelling results for data recorded by arrays CL and BR.

Our waveform modelling suggests a waveguide propagation distance of ∼5 km for all three faults. This value is compatible with the results obtained in the previous sections and is associated, as mentioned earlier, with a combination of along-strike and vertical components of the propagation path. If we assume for simplicity that the average along-strike and vertical components are the same, we get waveguides depth of ∼3.5 km. The other average estimated FZ properties for the CC fault are FZ width of ∼125 m, a reduced *S*-wave velocity relative to the host rock of approximately 35–45 per cent and *S*-wave quality factor of around 30–40. For fault CL, we obtain a width of ∼180 m, a reduced *S*-wave velocity relative to the host rock of 40 per cent, and *S*-wave quality factor of around 20–30. The corresponding results for fault BR are a width of ∼140 m, a reduced *S*-wave velocity relative to the host rock of approximately 30 per cent and *S*-wave quality factor of around less than 20. The width of the damage zone at the CC branch, with the highest quality of trapped wave recordings, is the narrowest among
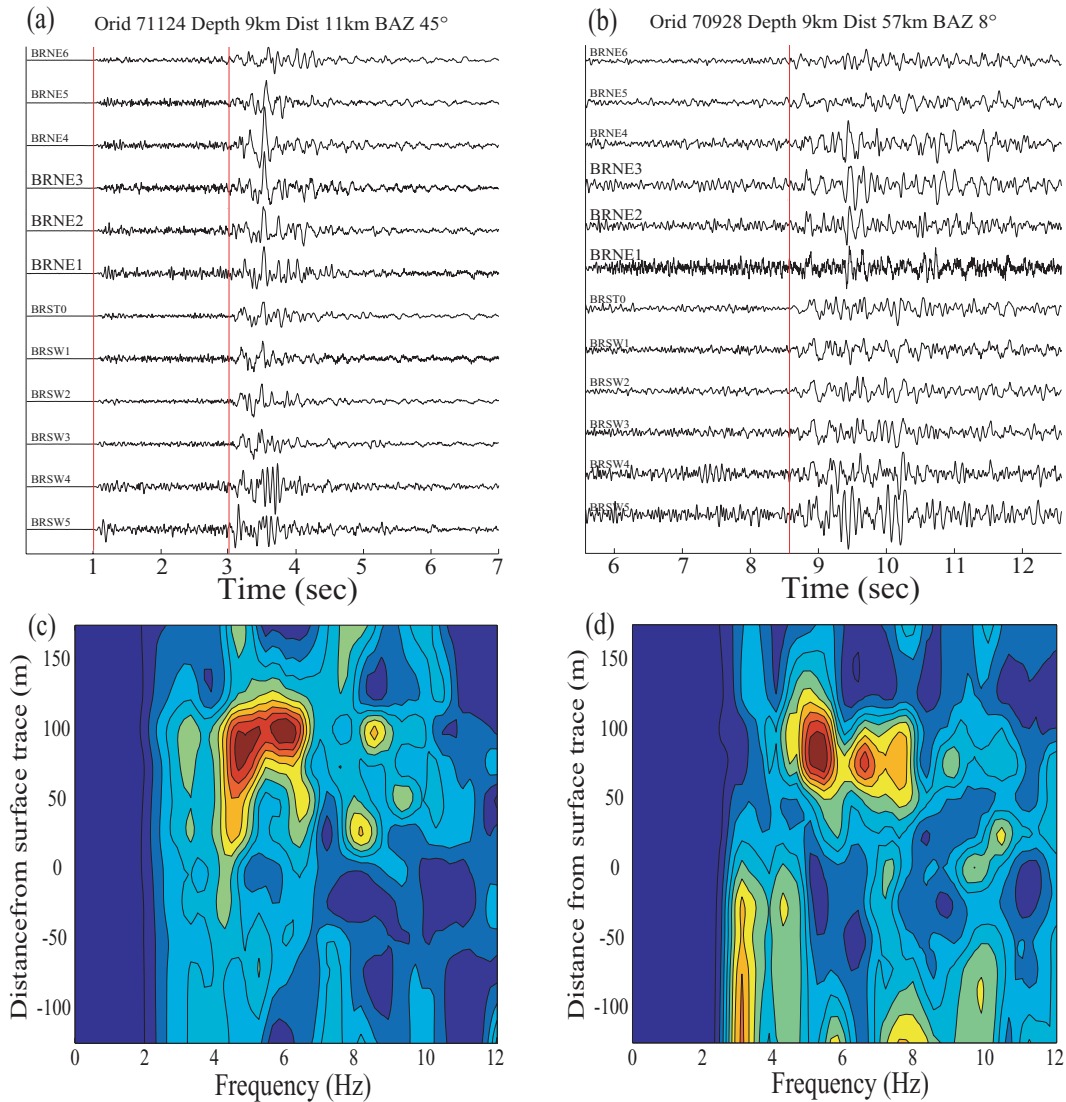
Figure 5. Examples of fault-parallel-component seismograms recorded at array BR and generated by events located relatively close to (a) and off (b) the fault. (c–d) Normalized amplitude spectra versus position of stations across array CL from waveforms shown in (a–b). Other notations are the same as in Fig. 3.

the three branches in the study area. The inversion results also indicate that the waveguides are not symmetric about the surface traces of the faults, but are offset to the northeast by 50–100 m. This can be seen directly from the waveform records of Figs 13–15 (and the results of Figs 3–5). Waveform inversions done for several other sets of seismograms recorded at each FZ array lead to similar overall results to those associated with Figs 13–15.

The flat regions with relatively high fitness values in some of the panels of Figs 13(b)–15(b) reflect the strong trade-offs that exist between the parameters governing the trapped waves (Ben-Zion 1998; Ben-Zion *et al.* 2003). We can, for example, fit the data well with larger FZ propagation distances if we adjust properly the values of FZ width, velocity and attenuation coefficient. This may explain why Li & Vernon (2001) were able to fit observed FZ trapped waves with a FZ layer that spans the entire seismogenic zone (although we note that they did not give quantitative measures for the fitting quality and parameter-space results as done in Figs 13–15). As mentioned above, waveform fits of FZ trapped cannot provide a unique image of the FZ structure because of the strong trade-offs between model parameters. For this reason, it is essential to obtain additional

constraints on the likely ranges of parameters from analysis of the spatial distribution of events generating trapped waves, and traveltime moveout of phases, as done here and our previous related studies (Ben-Zion *et al.* 2003; Peng *et al.* 2003).

3 DISCUSSION

We analysed waveform and traveltime data from a set of ~500 events recorded on three linear arrays across the CC, CL and BR branches of the SJFZ. We first assign a quality to the FZ trapped waves generation based on a spectral ratio method. Many events, including some clearly off the fault, have a high value of trapped wave quality, indicating that the trapping structures are shallow (Igel *et al.* 2002; Ben-Zion *et al.* 2003; Fohrmann *et al.* 2004). This interpretation is further supported by a lack of moveout for the time delays between the *S* wave and trapped wave group with increasing propagation distance. The average time delay between the *S* and trapped waves gives a total propagation distance in the FZ waveguide of less than 5 km, suggesting a waveguide depth of about 3.5 km.
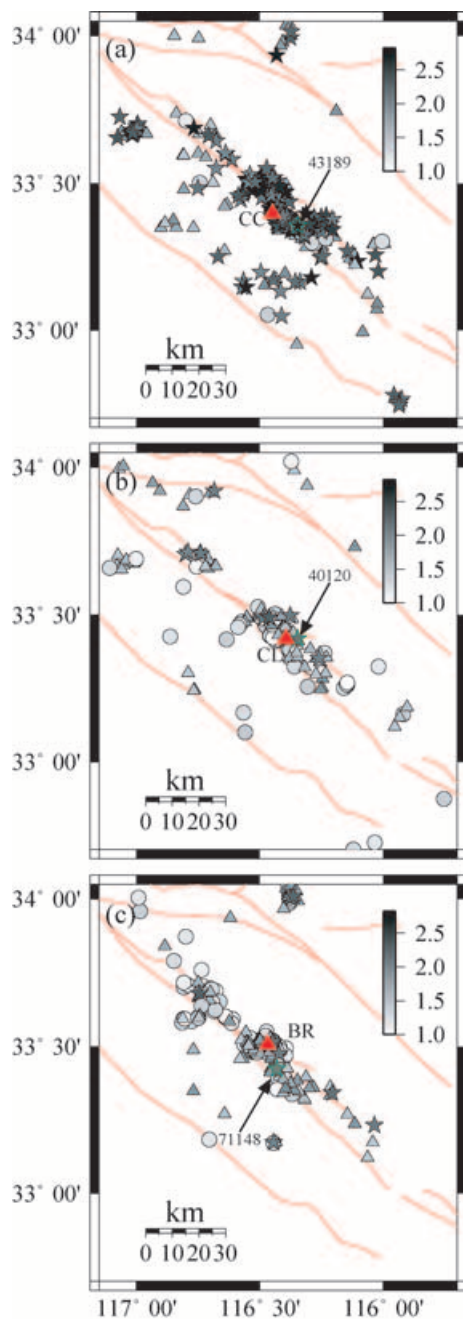
Figure 6. Maps of the events showing the calculated quality of the trapped waves recorded at array CC (a), CL (b) and BR (c). The shading represents the value of the assigned quality with darker representing higher values, and thus larger trapped waves. The top 25 per cent, middle 50 per cent and bottom 25 per cent of the spectral ratios for all of the data are assigned quality A, B and C for FZ trapped wave generation, and are marked as stars, triangles and circles, respectively. The fault surface traces are marked as thin lines and the location of the array as a large red triangle. Waveforms generated by events that are pointed to by arrows and highlighted are used in waveform modelling, Figs 13–15.

The synthetic waveform modelling provides additional information on the depth and other properties of the trapping structure. The total propagation distance calculated by the GIA for each fault is ∼5 km, compatible with the traveltime analysis and waveguide depth of 3–5 km.
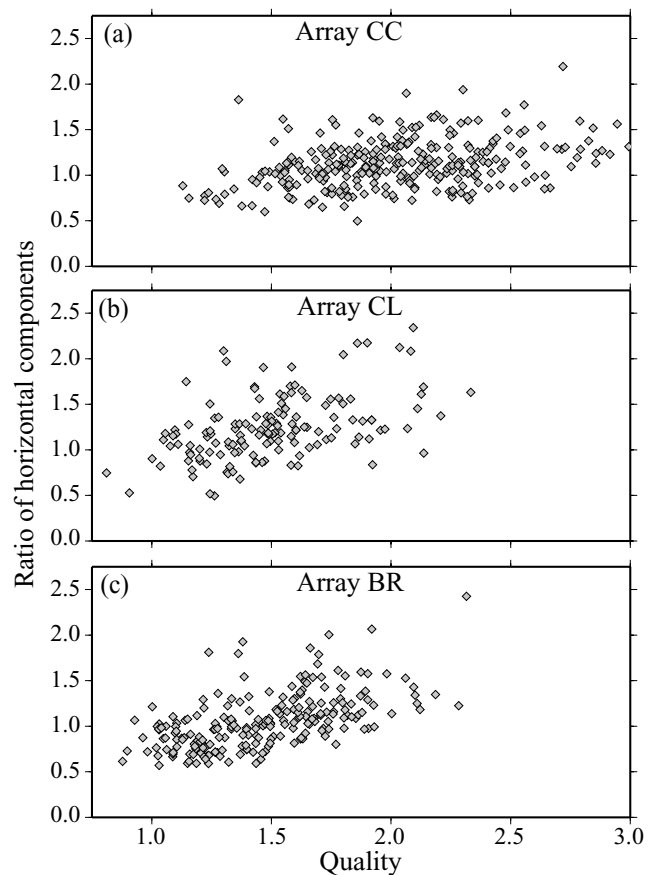

Figure 7. The ratio between fault-parallel and fault-perpendicular components plotted against the quality of the trapped wave generation for the events recorded at array CC (a), CL (b) and BR (c).

The inversion results indicate that the waveguide at each fault is not centred on the surface trace, but is offset by 50–100 m to the northeast. Interestingly, detailed geological mapping of the SJFZ at Anza show that the surface structure of the FZ has a similar asymmetry at a scale of metres, with the gouge and host rock to the northeast of the principal slip zone having considerably more damage than the corresponding rock units to the southwest (Dor *et al.* 2005). These asymmetric patterns of damaged rocks across the main traces of the faults may result from a preferred northwest propagation direction of earthquake ruptures on the SJFZ (Ben-Zion & Shi 2005, and references therein). Such a preferred propagation direction may, in turn, result from a velocity contrast across the SJFZ (e.g. Weertman 1980; Andrews & Ben-Zion 1997), with the northeast side having higher seismic velocities. Local traveltime tomography in the Anza area (Scott *et al.* 1994) and regional imaging studies (Magistrale & Sanders 1995; Shapiro *et al.* 2005) show that this is indeed the case. The analysis of trapped waves is not sensitive to a small velocity contrast between the crustal blocks on the opposite sides of the SJFZ, but such a contrast can have significant implications for many aspects of earthquake dynamics (e.g. Ben-Zion 2001, and references therein). It is therefore important to obtain in future studies stronger constraints on the velocity contrast across the SJFZ from detailed tomography (e.g. Thurber *et al.* 2004) and analysis of FZ head waves that refract along material interfaces in the FZ structure (e.g. Ben-Zion *et al.* 1992; McGuire & Ben-Zion 2005).

In various recent studies, similar shallow trapping structure have been found in the Karadere-Düzce branch of the NAF (Ben-Zion
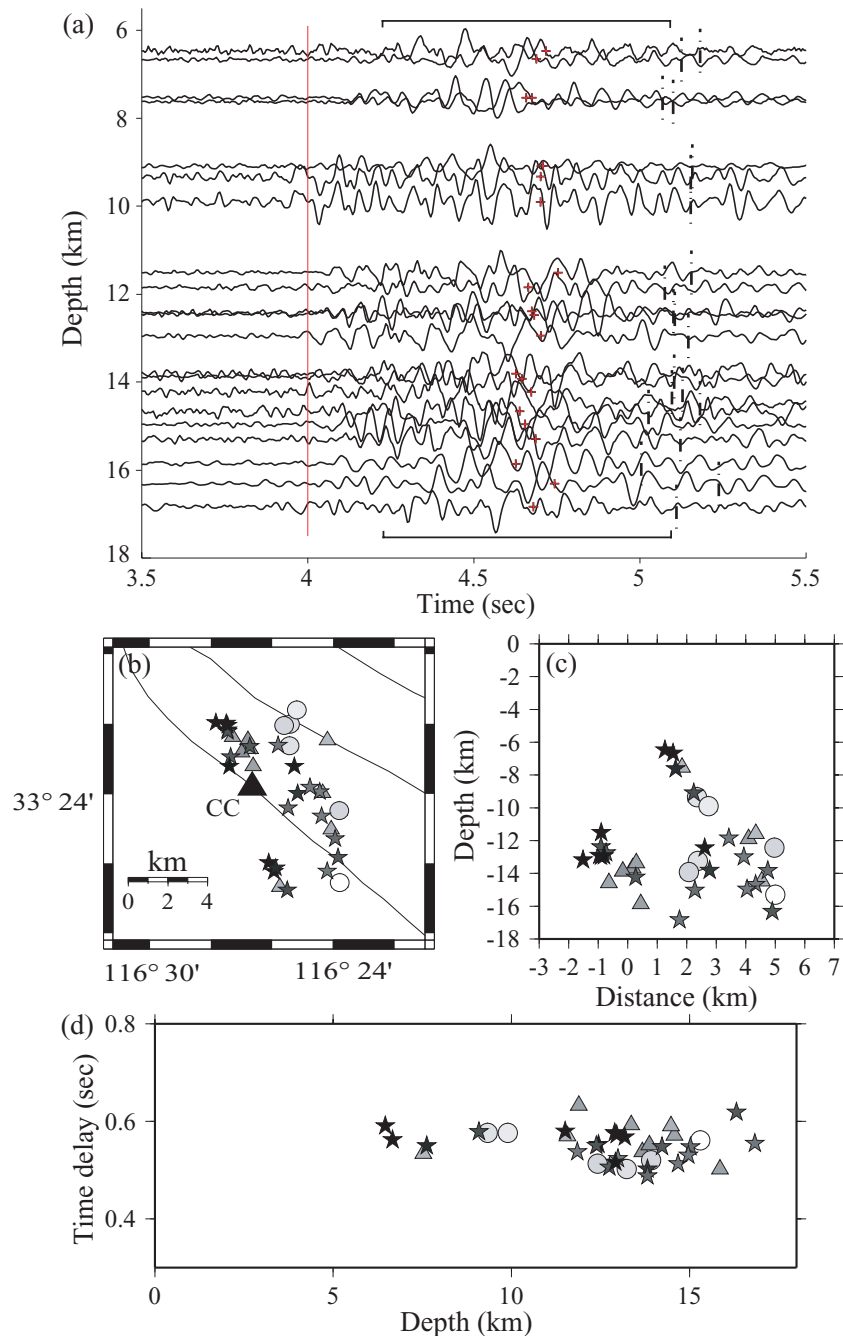
Figure 8. (a) Fault-parallel seismograms at station CCNE1 for 20 events with trapped wave quality A. The waveforms are aligned by their *S* waves at 4 s and marked by a red line. The horizontal bars above and below the seismograms bracket the trapped wave energy and the plus signs show the estimated trapped wave group centre. The vertical dashed lines mark the picked end of the trapped wave group. The events that produce these seismograms are a subset of the highest quality events, located within 5 km of the station. (b) The location of all the events within 5 km of array CC. The waveforms generated by the events marked by stars (quality A) are shown in (a). The shading and symbols represent the quality as described for Fig. 6. (c) Hypocentres projected on a cross-section perpendicular to the CC fault. (d) Time delay between the *S* arrivals and the mid point of the trapped waves group plotted against their depth for the events in (b).

et al. 2003), the Parkfield segment of the SAF (Michael & Ben-Zion 1998; Korneev *et al.* 2003), the rupture zone of the Landers earthquake (Peng *et al.* 2003) and an inactive FZ near Norcera Umbra, central Italy (Rovelli *et al.* 2002). This wide global distribution of faults with shallow trapping waveguides indicates that it is a common element of FZ structures. The fact that such a structure exists in inactive FZ (Rovelli *et al.* 2002) implies that the shallow FZ waveg-

uide is a long-lasting structure. Ben-Zion *et al.* (2003) suggested that the shallow trapping waveguide corresponds to the top part of a flower-type structure that is mechanically stable and is associated with relatively broad zone of deformation. This interpretation is supported by recent observations of shallow crustal anisotropy (3–4 km) around the rupture zone of 1999 Hector mine, California, earthquake (Cochran *et al.* 2003), near the 1999 Chi-Chi, Taiwan, earthquake
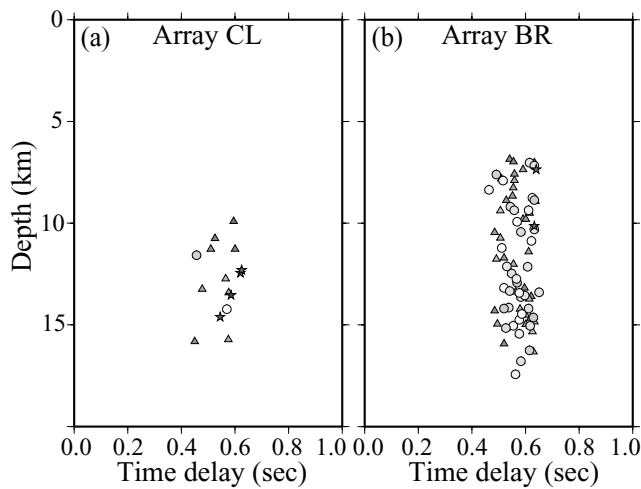
Figure 9. Time delay between the *S* arrival and the mid point of the trapped wave group plotted against the depths for a subset of events located directly under array CL (a), BR (b). The shading and symbols represent the quality as described for Fig. 6.

(Liu *et al.* 2004), and along the Karadere-Düzce branches of the North Anatolia fault (Peng & Ben-Zion 2004). Since the observed FZ trapped waves (and anisotropy) are dominated by the upper 3–4 km of the shallow crust, the results do not provide in general information on properties of the FZ structure at seismogenic depth, where earthquakes nucleate and the bulk of seismic slip occurs.

Ben-Zion & Aki (1990) showed with analytical model calculations that a low-velocity FZ layer with realistic parameters can produce motion amplification of factor 30 and more in the vicinity of the fault. Cormier & Spudich (1984) and Spudich & Olsen (2001) found a large amplification for 0.6–1.0 Hz waves within ∼1–2 km wide low-velocity zone around the rupture of the 1984 Morgan Hill earthquake. Seeber *et al.* (2000) observed a factor 5 amplification of acceleration in a station located in the rupture zone of the 1999 Izmit earthquake on the Karadere branch of the NAF with respect to nearby off-fault station. Rovelli *et al.* (2002) reported large amplification of ground motion at stations inside an inactive fault for an $M_W = 5.3$ subcrustal earthquake occurred at a depth of 48 km and an epicentral distance of 10 km from Nocera Umbra, Italy. Davis *et al.* (2000) reported an anomalously concentrated damage around the city of Santa Monica during the 1994 Northridge, California earthquake, and interpreted it as a focusing of seismic waves by subsurface faults. In this study, we found shallow (∼ 3–5 km) and ∼100 m wide waveguides that can trap seismic energy generated by earthquakes clearly outside the FZ. Because of the large volume of potential sources that can produce motion amplifications around shallow FZ waveguides, such structures can have important implications for seismic shaking hazard (e.g. Spudich & Olsen 2001; Ben-Zion *et al.* 2003; Fohrmann *et al.* 2004).

The numerical simulations of Fohrmann *et al.* (2004) indicate that the volume of sources capable of generating trapped waves at shallow waveguide structures increases with the hypocentral depth, and that the amount of observed trapped energy depends on the source types (e.g. orientation of the rupture plane and slip direction) and receiver position within the radiation pattern of the sources. The SJFZ is a complex structure with many discontinuities and subsidiary faults (e.g. Sanders & Kanamori 1984; Sanders & Magistrale 1997). The focal mechanisms of earthquakes around the SJFZ are highly diverse (e.g. Hauksson 2000), and the event depths are in the
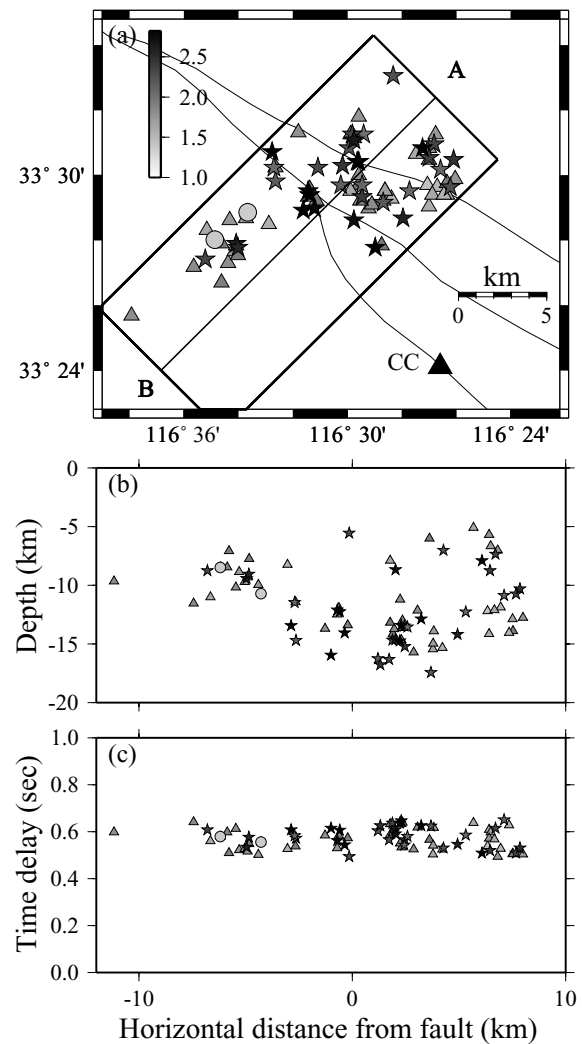

Figure 10. (a) Quality of trapped waves generation for a subset of events across the FZ in the box A–B and recorded at array CC (large triangle). Other symbols are the same as in Fig. 6. (b) Hypocentres projected from the box along the cross-section A–B. (c) Time delay between the S arrivals and the mid point of the trapped waves group plotted against the distances from the fault.

range of ∼5–20 km. The large diversity of focal mechanisms and range of event depths explain why many earthquakes in our study area are capable of producing trapped waves in the FZ stations. A similar situation was found to exist along the Karadere-Düzce branch of the North Anatolian fault (Ben-Zion *et al.* 2003), and to a somewhat lesser extent also along the rupture zone of the 1992 Landers earthquake (Peng *et al.* 2003).

The obtained FZ width of ∼100 m is associated with observations of FZ trapped waves that are in the frequency range of ∼2–10 Hz, and produced by microearthquakes, typically less than magnitude 3. The width associated with FZ amplification during a major earthquake can be much larger than ∼100 m, because of the relative low-frequency seismic waves radiated by large earthquakes (e.g. Spudich & Olsen 2001). On the other hand, non-linear amplification effects (e.g. Field *et al.* 1997) may reduce the level of shaking inside the FZ during a major earthquake. The above issues should be addressed when extrapolating the results of FZ trapped waves generated by microearthquakes to evaluate the likely amplification that
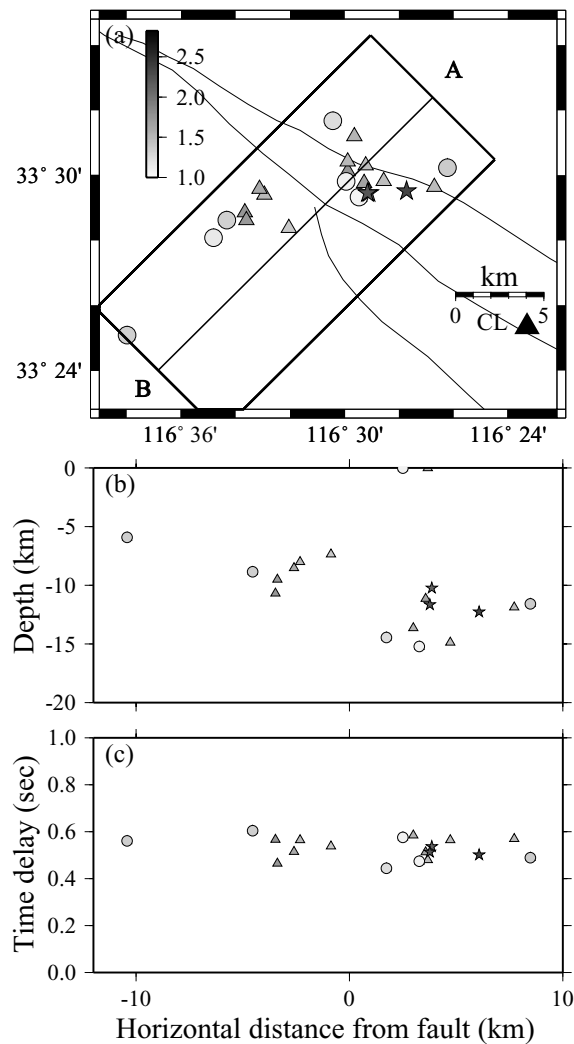
Figure 11. (a) Quality of trapped waves generation for a subset of events across the FZ in the box A–B and recorded at array CL (large triangle). Other symbols are the same as in Fig. 6. (b) Hypocentres projected from the box along the cross-section AB. (c) Time delay between the *S* arrivals and the mid point of the trapped waves group plotted against the distances from the fault. (Same as in Fig. 10).
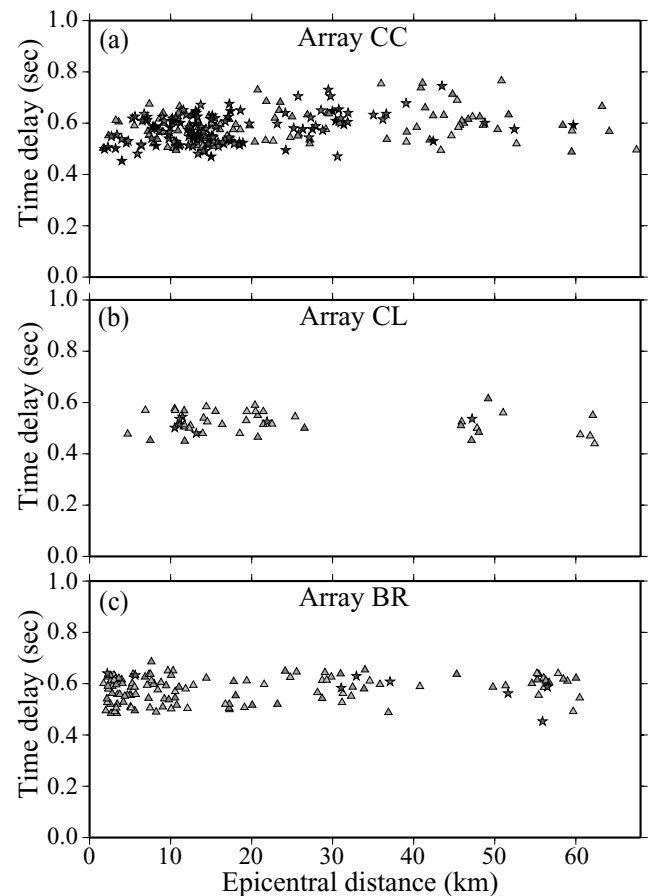

Figure 12. Time delay between the *S* arrival and the mid point of the trapped wave group plotted against distance for events recorded at array CC (a), CL (b) and BR (c). The shading denotes the spectral ratio between FZ trapped waves and *S* waves. Stars and triangles denote quality A and B, respectively.

can be generated by a FZ during a major earthquake (e.g. Michael *et al.* 2002).

REFERENCES

Andrews, D.J. & Ben-Zion, Y., 1997. Wrinkle-like Slip Pulse on a Fault between Different Materials, *J. geophys. Res.,* **102,** 553–571.

Ben-Zion, Y., 1998. Properties of seismic fault zone waves and their utility for imaging low velocity structure, *J. geophys. Res.,* **103,** 12 567–12 585.

Ben-Zion, Y., 2001. Dynamic Rupture in Recent Models of Earthquake Faults, *J. Mech. Phys. Solids,* **49,** 2209–2244.

Ben-Zion, Y. & Aki, K., 1990. Seismic radiation from an SH line source in a laterally heterogeneous planar fault zone, *Bull. seism. Soc. Am.,* **80,** 971–994.

Ben-Zion, Y., Katz, S. & Leary, P., 1992. Joint inversion of fault zone head waves and direct P arrivals for crustal structure near major faults, *J. geophys. Res.,* **97**(2), 1943–1951.

Ben-Zion, Y. *et al.*, 2003. A shallow fault zone structure illuminated by trapped waves in the Karadere-Düzce branch of the north Anatolian Fault, Western Turkey, *Geophys. J. Int.,* **152,** 699–717.

Ben-Zion, Y. & Sammis, C.G., 2003. Characterization of fault zones, *Pure appl. Geophys.,* **160,** 677–715.

Ben-Zion, Y. & Shi, Z., 2005. Dynamic rupture on a material interface with spontaneous generation of plastic strain in the bulk, *Earth. Plant. Sci. Lett.,* in press.

Berger, J., Baker, L.N., Brune, J.N., Fletcher, J.B., Hanks, T.C. & Vernon, F.l., 1984. The Anza array: a high dynamic-range, broad-band, digitally radio-telemetered seismic array, *Bull. seism. Soc. Am.,* **74,** 1469–1682.

Crase, E., Pica, A., Noble, M., McDonald, J. & Tarantola, A., 1990. Robust elastic non-linear inversions: applications to real data, *Geophysics,* **55,** 527–538.

Cormier, V.F. & Spudich, P., 1984. Amplification of ground motion and waveform complexities in fault zones: examples from the San Andreas and the Calaveras faults, *Geophys. J. R. Astron. Soc.,* **79,** 135–152.

Cochran, E.S., Vidale, J.E. & Li, Y.-G., 2003. Near-fault anisotropy following the Hector Mine earthquake, *J. geophys. Res.,* **108,** 2436, doi:10.1029/2002JB002352.
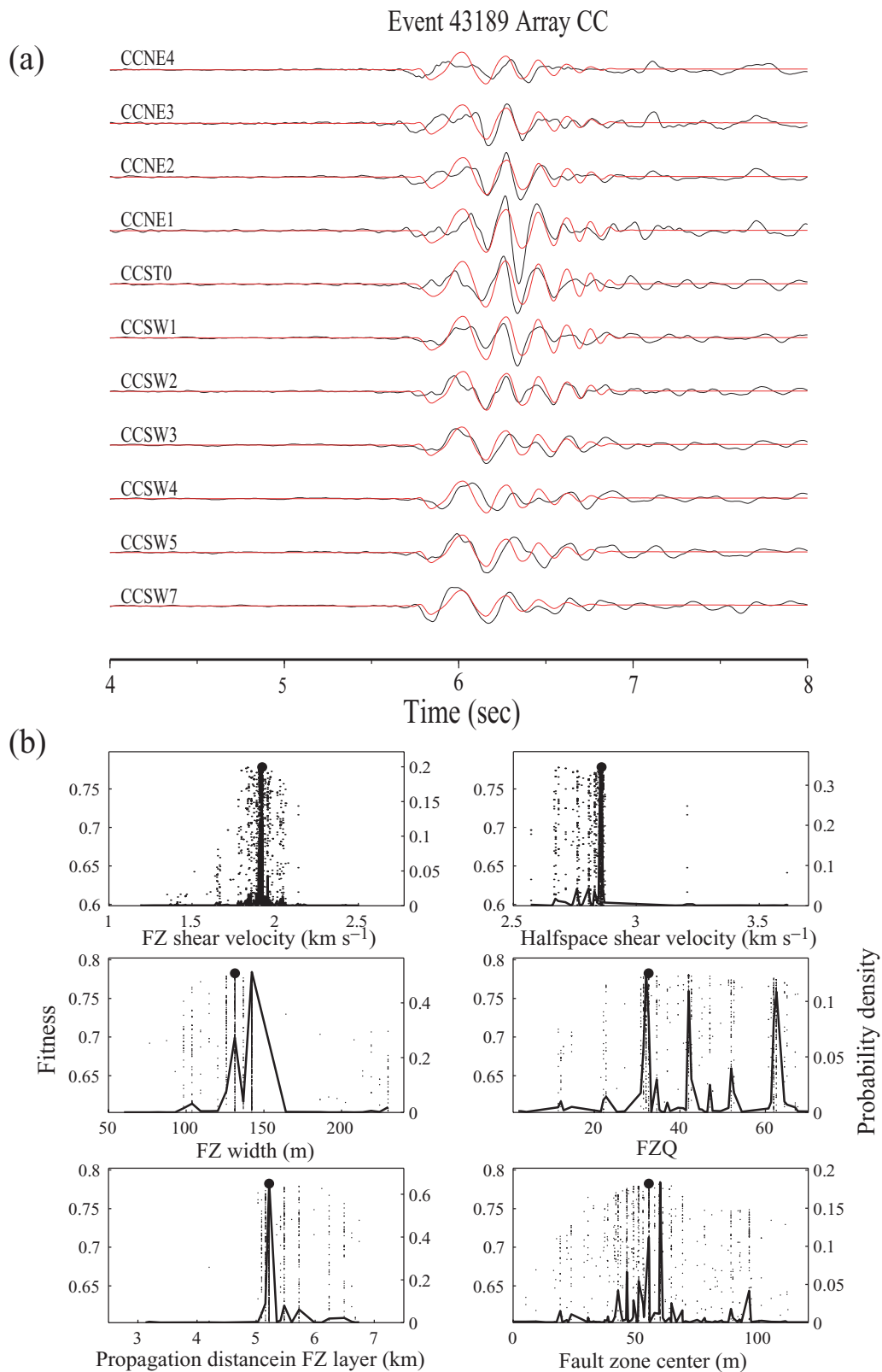
Figure 13. (a) Synthetic (red lines) waveform fit of fault-parallel displacement seismograms (dark lines) at array CC for the event located in Fig. 6(a). (b) Fitness values (dots) associated with different FZ parameters tested by the genetic inversion algorithm. The model parameters associated with the highest fitness values (solid circles) were used to generate the synthetic waveforms in (a). The curves give probability density functions for the various model parameters.

Figure 14. (a) Synthetic (red lines) waveform fits of fault-parallel displacement seismograms (dark lines) at array CL for the event located in Fig. 6(b). (b) Fitness values (dots) associated with different FZ parameters tested by the genetic inversion algorithm for array. The model parameters associated with the highest fitness values (solid circles) were used to generate the synthetic waveforms in (a). The curves give probability density functions for the various model parameters.
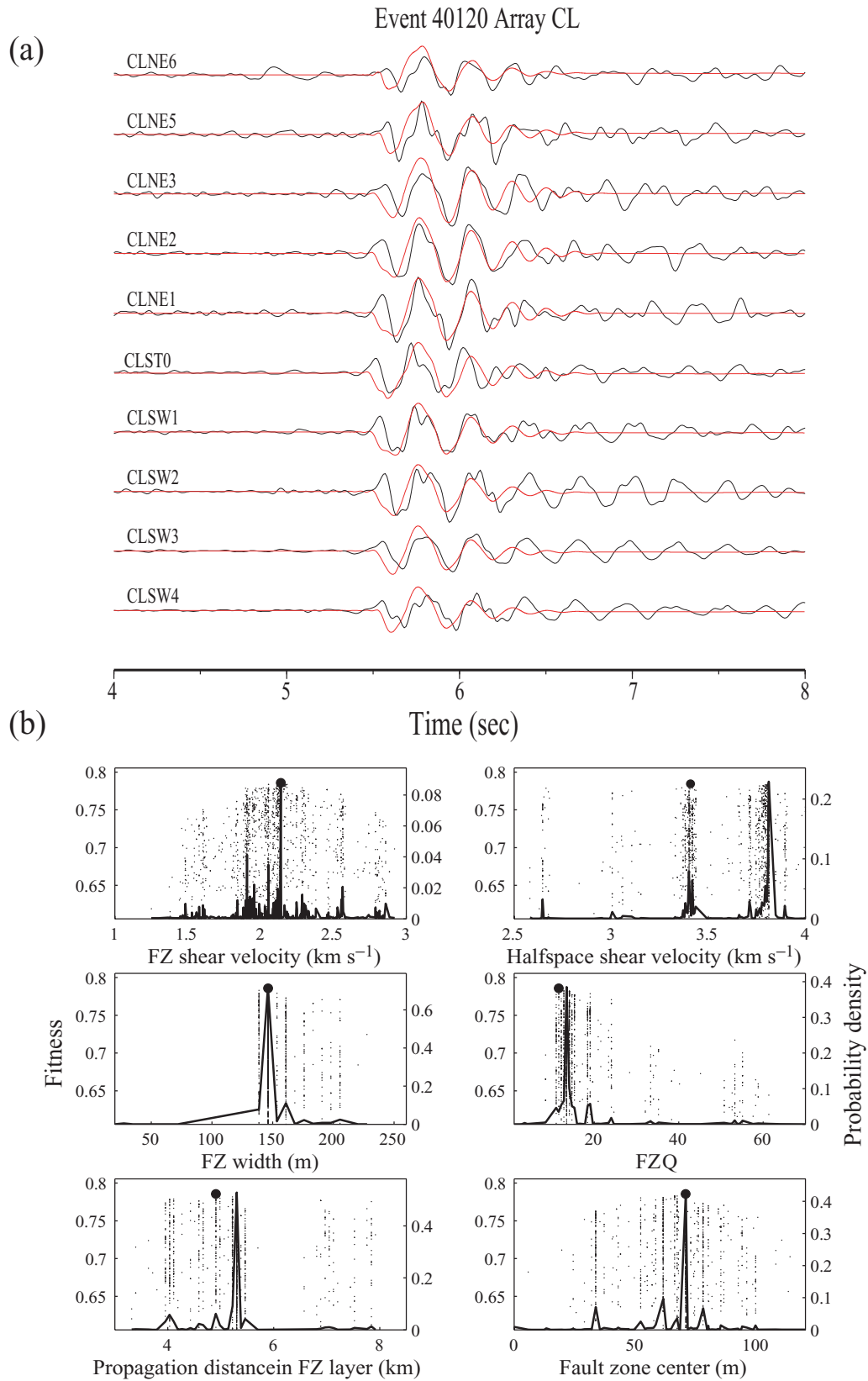
Figure 15. (a) Synthetic (red lines) waveform fits of fault-parallel displacement seismograms (dark lines) at array BR for the event located in Fig. 6(c). (b) Fitness values (dots) associated with different FZ parameters tested by the genetic inversion algorithm. The model parameters associated with the highest fitness values (solid circles) were used to generate the synthetic waveforms in (a). The curves give probability density functions for the various model parameters.
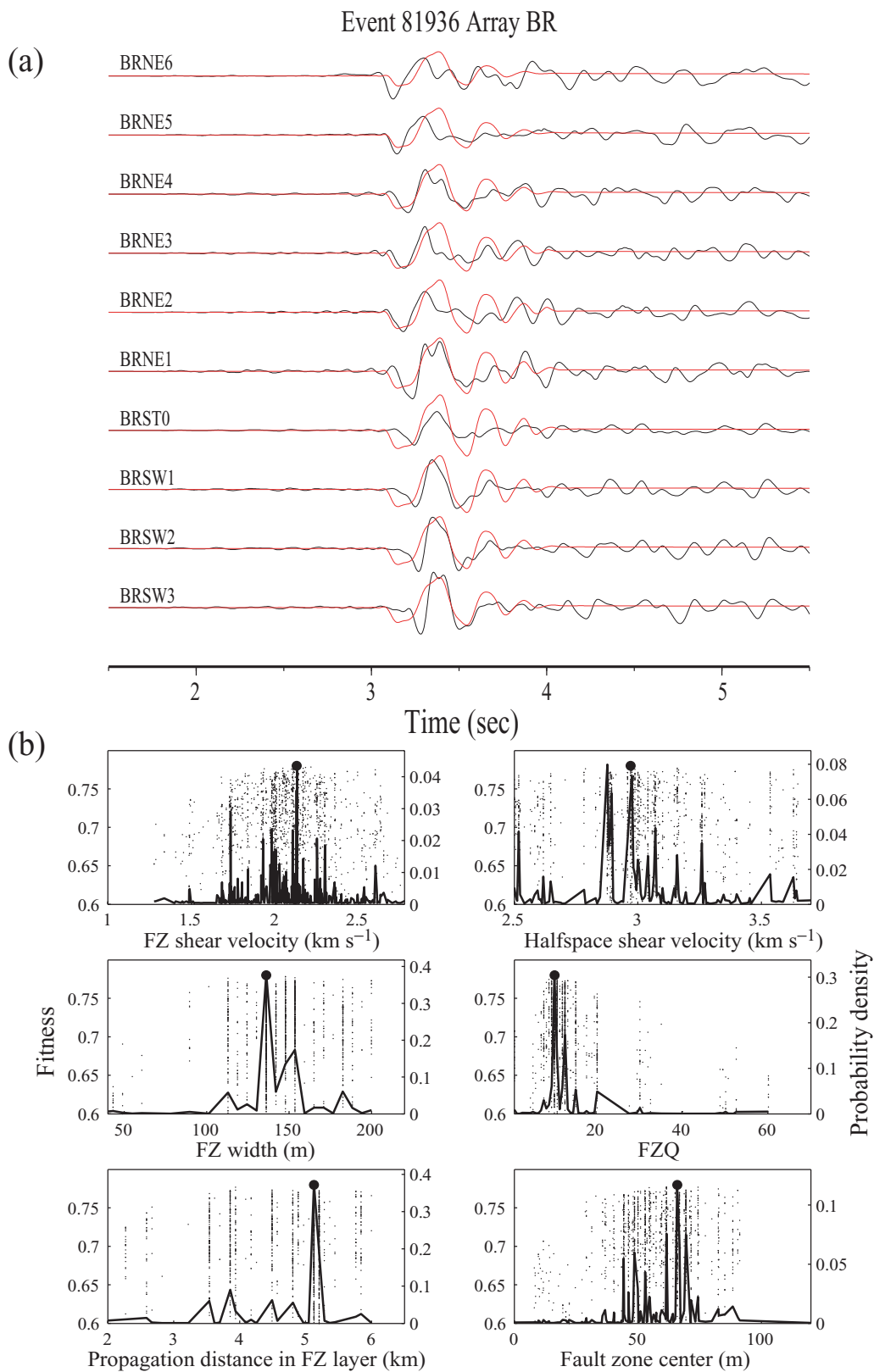
Davis, P.M., Rubinstein, J.L., Liu, K.H., Gao, S.S. & Knopoff, L., 2000. Northridge earthquake damage caused by geologic focusing of seismic waves, *Science,* **289,** 1746–1750.

Dor, O., Rockwell, T. & Ben-Zion, Y., 2005. Geologic observations of damage asymmetry in the structure of the San Jacinto, San Andreas and Punchbowl faults in southern California: A possible indicator for preferred rupture propagation direction, submitted to *Pure appl. Geophys.*

Fletcher, J., Haar, L., Hanks, T., Baker, L., Vernon, F., Berger, J. & Brune, J., 1987. The digital array at Anza, California: Processing and initial interpretation of source parameters, *J. geophys. Res.,* **92,** 369–382.

Field, E.H., Johnson, P.A., Beresnev, I.A. & Zeng, Y., 1997. Nonlinear ground-motion amplification by sediments during the 1994 Northridge earthquake, *Nature,* **390,** 599–602.

Fohrmann, M., Jahnke, G., Igel, H. & Ben-Zion, Y., 2004. Guided waves from sources out side faults: an indication of shallow trapping structure? *Pure appl., Geophys.,* **161,** 2125–2137.

Haberland, C. *et al.*, 2003. Modeling of seismic guided waves at the Dead Sea Transform, *J. geophys. Res.,* **108,** 2342, doi:10.1029/2002JB002309.

Hauksson, E., 2000. Crustal structure and seismicity distribution adjacent to the Pacific and North America plate boundary in southern California, *J. geophys. Res.,* **105,** 13 875–13 903.

Igel, H., Ben-Zion, Y. & Leary, P., 1997. Simulation of SH and P-SV wave propagation in fault zones, *Geophys. J. Int.,* **128,** 533–546.

Igel, H., Jahnke, G. & Ben-Zion, Y., 2002. Numerical simulation of fault zone guided waves: accuracy and 3-D effects, Pure *appl. Geophys.,* **159,** 2067–2083.

Jahnke, G., Igel, H. & Ben-Zion, Y., 2002. 3-D calculations of fault zone guided waves in various irregular structures, *Geophys. J. Int.,* **151,** 416–426.

Korneev, V.A., Nadeau, R.M. & McEvilly, T.V., 2003. Seismological Studies at Parkfield IX: Fault-one imaging using Guided Wave Attenuation, *Bull. Seism. Soc. Am.,* **93,** 1415–1426.

Li, Y.-G. & Leary, P.C., 1990. Fault zone trapped waves, *Bull. seism. Soc. Am.,* **80**(5), 1245–1271.

Li, Y.-G., Leary, P.C., Aki, K. & Malin, P., 1990. Seismic trapped modes in the Orville and San Andreas Fault zones, *Science,* **249,** 763–766.

Li, Y.-G., Vidale, J.E. & Aki, K., 1997. San Jacinto fault zone guided waves: a discrimination for recently active fault strands near Anza, California, *J. geophys. Res.,* **102,** 11 689–11 701.

Li, Y.-G. & Vernon, F.L., 2001. Characterization of the San Jacinto fault zone near Anza, California, by fault zone trapped waves, *J. geophys. Res.,* **106,** 30 671–30 688.

Liu, Y., Teng, T.-L. & Ben-Zion, Y., 2004. Systematic analysis of shear-wave splitting in the aftershock zone of the 1999 Chi-Chi earthquake: shallow crustal anisotropy and lack of precursory variations, *Bull. Seismol. Soc. Am.,* **94,** 2330–2347.

Magistrale, H. & Sanders, C., 1995, P wave image of the Peninsular Ranges batholith, southern California, *Geophys. Res. Lett.,* **22,** 2549–2552.

Marra, F., Azzara, R., Bellucci, F., Caserta, A., Cultrera, G., Mele, G., Palombo, B., Rovelli, A. & Boschi, E., 2000. Large amplification of ground motion at rock sites within a fault zone in Nocera Umbra (Central Italy), *J. Seism.,* **4,** 534–554.

McGuire, J. & Ben-Zion, Y., 2005. High-resolution imaging of the Bear Valley section of the San Andreas Fault at seismogenic depths with fault-zone head waves and relocated seismicity, *Geophys. J. Int.,* doi:10.1111/j.1365-246X.2005.02703.x.

Michael, A.J. & Ben-Zion, Y., 1998. Inverting Fault Zone Trapped Waves with Genetic Algorithm, *EOS, Trans. Am. geophys, Un.,* **79,** F584.

Michael, A.J., Ross, S.L. & Stenner, H.D., 2002. Displaced rocks, strong motion, and the mechanics of shallow faulting associated with the 1999 Hector Mine, California, earthquake, *Bull. seism. Soc. Am.,* **92,** 1561–1569.

Mizuno, T., Nishigami, K., Ito, H. & Kuwahara Y., 2004. Deep structure of the Mozumi-Sukenbu fault, central Japan, estimated from the subsurface array observation of the fault zone trapped waves, *Geophys. J. Int.,* **159,** 622–642.

Mori, J., 1993. Fault plane determinations for three small earthquakes along the San Jacinto fault, California: search for cross faults, *J. geophys. Res.,* **98,** 17 711–17 722.

Peng, Z. & Ben-Zion, Y., 2004. Systematic analysis of crustal anisotropy along the Karadere-Düzce branch of the north Anatolian fault, *Geophys. J. Int.,* **159,** 253–274.

Peng, Z., Ben-Zion, Y., Zhu, L. & Michael, A.J., 2003. Inference of a shallow fault zone layer in the rupture zone of the 1992. Landers, California earthquake fro locations of events generating trapped waves and traveltime analysis, *Geophys. J. Int.,* **155,** 1021–1041.

Rovelli, A., Caserta, A., Marra, F. & Ruggiero, V., 2002. Can seismic waves be trapped inside an inactive fault zone? The case study of Nocera Umbra, central Italy, *Bull. seism. Soc. Am.,* **92,** 2217–2232.

Sanders, C.O. & Kanamori, H., 1984. A seismo-tectonic analysis of the Anza seismic gap, San Jacinto fault zone, southern California, *J. geophys. Res.,* **89,** 873–875, 890.

Sanders, C.O. & Magistrale, H., 1997. Segmentation of the northern San Jacinto fault zone, southern California, *J. geophys. Res.,* **102,** 27 453–27 467.

Seeber, L., Armbruster, J.G., Ozer, N., Aktar, M., Baris, S., Okaya, D., Ben-Zion, Y. & Field, E., 2000. The 1999 Earthquake Sequence along the North Anatolia Transform at the Juncture between the Two Main Ruptures, in *The 1999 Izmit and Duzce Earthquakes: Preliminary Results*, pp. 209–223, eds Barka et al Istanbul technical university.

Scott, J.S., Masters, T.G. & Vernon, F.L., 1994. 3-D velocity structure of the San Jacinto Fault zone near Anza, California, *Geophys. J. Int.,* **119,** 611–626.

Sharp, R.J., 1967. San Jacinto fault zone in the peninsular ranges of southern California, *Geol. Soc. Am. Bull.,* **78,** 705–730.

Shapiro, N.M., Campillo, M., Stehly, L. & Ritzwoller, M.H., 2005. High resolution surface wave tomography from ambient seismic noise, *Science*, **307,** 1615–1618.

Spudich, P. & Olsen, K.B., 2001. Fault zone amplified waves as a possible seismic hazard along the Calaveras fault in central California, *Geophys. Res. Lett.,* **28,** 2533–2536.

Thurber, C., Roecker, S., Zhang, H., Baher, S. & Ellsworth, W., 2004. Fine-scale structure of the San Andreas fault and location of the SAFOD target earthquakes, *Geophys. Res. Lett.,* **31,** L12S02, doi:10.1029/2003GL019398.

Vidale, J.E., Helmberger, D.V. & Clayton, R.W., 1985. Finite-difference seismograms for SH waves, *Bull. seism. Soc. Am.,* **75,** 1765–1782.

Wagner, G.S., 1998. Local wave propagation near the San Jacinto fault zone, Southern California: observations from a three component seismic array, *J. geophys. Res.,* **103,** 7231–7246.

Weertman, J.J., 1980. Unstable slippage across a fault that separates elastic media of different elastic constants, *J. geophys. Res.,* **85,** 1455–1461.